ACS APPLIED MATERIALS & INTERFACES

Research Article

www.acsami.org

Mechanisms Counteracting the Growth of Large Grains in Industrial ZnS Grown by Chemical Vapor Deposition

T. Zscheckel,[†] W. Wisniewski,*[,†] A. Gebhardt,[‡] and Christian Rüssel[†]

[†]Otto-Schott-Institut, Jena University, Fraunhoferstr. 6, 07743 Jena, Germany

[‡]VITRON GmbH, am Nasstal 5, 07752 Jena, Germany

ABSTRACT: Polycrystalline ZnS produced by chemical vapor deposition (CVD) is analyzed using X-ray diffraction (XRD) and scanning electron microscopy (SEM) including electron backscatter diffraction (EBSD) to gain insight into the growth mechanism. Epitaxial growth of ZnS (111) layers is indicated in cubic CVD-ZnS. Mechanisms counteracting the growth of large, homogeneously oriented grains are proposed. This includes the summation of faults at low-angle grain boundaries during the deposition of new layers as well as the formation of new growth directions perpendicular to the sides of large grains. Wurtzite could be identified as a product of instable deposition conditions at the beginning and end of the deposition process.

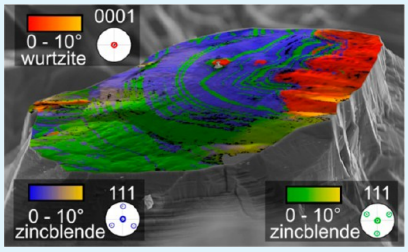

KEYWORDS: *CVD-ZnS, grain growth, epitaxial growth, twinning, EBSD*

INTRODUCTION

Polycrystalline materials for photonic applications have recently gained substantial interest as they offer properties which cannot be achieved by optical glasses. ZnS with its large band gap of 3.72 eV[1] and "a nearly free electron band structure in a zincblende crystal"[2] enables a transparency between 380 nm and 10.5 μm.[3] It may be used for optical infrared components of up to 30 mm thickness. An industrial chemical vapor deposition (CVD) process enables us to utilize ZnS as a bulk material of high purity. It differs notably from the processes used to obtain thin ZnS CVD films. ZnS grows from H_2S gas and zinc vapor in the industrial process, where several square meters of product are produced in large reaction chambers of more than 1 m^3 in volume during a process time of more than one week. The obtained material must be processed further before optical grade ZnS is obtained. Hence, a detailed understanding of the growth mechanisms during CVD may lead to higher product quality and lower production costs.

A recently published article has highlighted that the microstructural development during this CVD process is actually not understood very well. A significant growth selection in the early stages of deposition leads to increasing grain sizes and a nonuniform grain structure with an increasing distance from the substrate.[4] Texture formation and twinning are also observed in the CVD-ZnS layers.[4] However, some unknown mechanisms finally lead to the growth of a fine microstructure with internal stresses.[4] ZnS occurs in two phases: cubic zincblende (β-ZnS) and hexagonal wurtzite (α-ZnS). Zincblende is thermodynamically stable up to 1023 °C[5] and hence also the stable phase under the conditions supplied during the CVD process. Wurtzite is stable above 1023 °C, and a number of additional ZnS polytypes, differing in the stacking sequence of the close-packed polar layers,[6] have been described in the literature.[7,8] Both phases share the same density of 4.09 g/cm^3, calculated from crystallographic data.[9,10]

In this article, we focus on the ZnS layers grown during early deposition, when large, nonuniform grains are formed.[4] The phase composition and crystal orientation are examined using X-ray diffraction (XRD), scanning electron microscopy (SEM), and especially electron backscatter diffraction (EBSD).

EXPERIMENTAL APPROACH

Polycrystalline ZnS was produced via CVD from zinc vapor and H_2S gas at 680 °C in an industrial production process designed to produce ZnS layers with a thickness up to 35 mm with graphite as the substrate material (Vitron GmbH, Jena, Germany). To study the phase formation and the growth mechanisms at early stages of the process, the CVD process was stopped after only 10 h, although it would usually proceed for more than one week. All of the samples discussed in this article were taken from the same cycle.

The samples were studied by X-ray diffraction (XRD) using a Bruker D8 Discover diffractometer and Cu Kα radiation. Scanning electron microscopy (SEM) and electron backscatter diffraction (EBSD) were performed using a Jeol JSM-7001F equipped with a TSL Digiview 3 EBSD camera. Some samples were embedded in Araldite to improve handling during polishing. Surface charging in the SEM was avoided by contacting the samples with Ag paste and applying a thin layer of carbon at a pressure of about 10^{-3} Pa.

EBSD scans were captured and evaluated using the programs TSL OIM Data Collection 5.31 and TSL OIM Analysis 5.31. The EBSD scans were performed using a voltage of 20 kV. Only the fit-value was used for ranking the orientation solutions as this improved the certainty of phase discrimination in these studies. To increase the fraction of reliably indexed points, the scan data were cleaned by confidence index standardization with a grain tolerance angle of 1° and a minimum grain size of 5. Orientation data were not changed by this procedure. Afterward, only points with a confidence index (CI) $\geq$ 0.1 were considered in evaluations, indicating the attributed orientation solutions are correct with a probability of at least 96%.[11]

Received: October 10, 2013
Accepted: November 27, 2013
Published: November 27, 2013

RESULTS AND DISCUSSION

For a better understanding of the following results, it is helpful to keep in mind that all the samples used for this study were taken from the same industrial cycle.

Figure 1 shows XRD patterns recorded from various locations of the produced CVD-ZnS. A logarithmic scale is used for a better illustration of low intensity details and a better phase identification. The patterns represent data from the immediate interface to the graphite substrate (a), then from the immediate growth front (b), and finally from powdered material encompassing the entire thickness of the sample for comparison (c). The theoretical XRD patterns of wurtzite and zincblende are also presented (d). All the experimental patterns predominantly show peaks attributed to zincblende, but additional low intensity peaks of wurtzite are also observed. While the pattern from the immediate interface to the graphite substrate (a) shows clear {10$\bar{1}$0}, {10$\bar{1}$1}, {10$\bar{1}$2}, and {10$\bar{1}$3} peaks of wurtzite, the pattern from the growth front (b) shows only very weak {10$\bar{1}$0} and {10$\bar{1}$3} peaks. The pattern obtained from the powdered material does not indicate a clear presence of wurtzite.

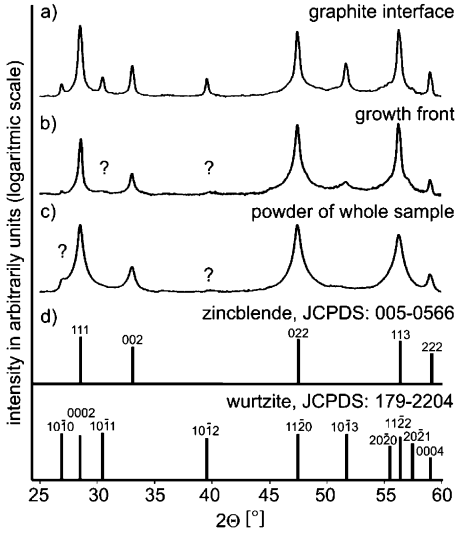

Figure 1. XRD patterns displayed using a logarithmic scale to highlight low intensity details in: (a) the intermediate interface to graphite substrate, (b) growth front, (c) powder of the whole deposited layer, and (d) theoretical XRD patterns of zincblende and wurtzite.

Cross sections of the material were cut and polished to locate the wurtzite phase indicated by XRD analyses. Figure 2 shows an SEM micrograph superimposed by combined inverse pole figure (IPF) and image quality (IQ) maps of the points indexed as zincblende in the area scanned by EBSD. The former position of the graphite substrate is indicated schematically. Most of the primary layers deposited adjacent to the substrate were torn out during the polishing process, but the remaining material is sufficient to confirm the existence of wurtzite and localize its position by EBSD as will be shown in Figure 3. Embedding the samples in a polymer can only reduce but not prevent this problem. The overall growth direction of ZnS is perpendicular to the substrate, i.e., from top to bottom in Figure 2. The sections 1, 2, and 3 framed in white are displayed in higher magnifications in Figures 3−5.

Figure 3 presents a combined IQ and phase map where data points indexed as zincblende are marked green, while wurtzite

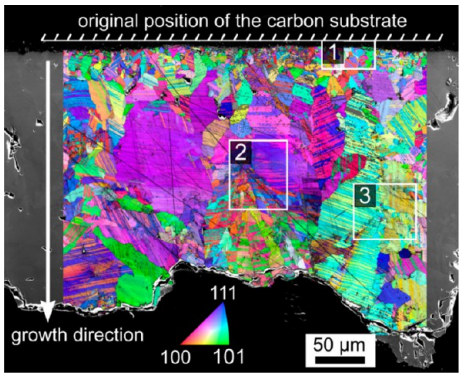

Figure 2. SEM micrograph of a sample cut perpendicular to the substrate superimposed by combined IPF and IQ maps of EBSD scans performed on the area. The data show the entire thickness of the deposited layer resulting from an interrupted process. The framed areas 1−3 are featured in the subsequent Figures 3−5 in greater detail.

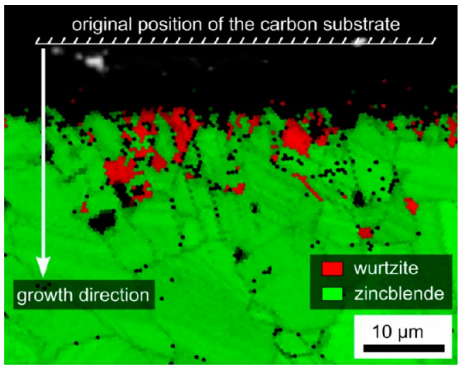

Figure 3. Combined phase and IQ map of the area 1 framed in Figure 2.

is marked red. Data points with a low pattern quality receive a lower grayscale value and appear darker, e.g., at grain boundaries, while unreliably indexed patterns appear black. Wurtzite is localized to a number of small grains in the topmost ZnS layers close to the former substrate.

As expected from previous results[4] and the XRD results of Figure 1, Figures 2 and 3 confirm that wurtzite does not occur in the bulk. The size of the zincblende grains increases as growth proceeds. Large, nonuniform grains with a high frequency of lamellae-shaped twins are observed. These large grains form the growth front of ZnS during the time period before the fine grained growth observed 1 mm from the surface[4] occurs, i.e., roughly 8−10 h into the CVD process.

Although ZnS may theoretically react to solid ZnO and gaseous H_2S in an oxygen-containing atmosphere, ZnO is neither indicated by XRD nor EDX analyses in the SEM. Additionally, hexagonal ZnO could easily be distinguished from the cubic zincblende by EBSD where the information depth is in the nanometer scale; i.e., a thin surface layer would not go unnoticed. Although ZnO and wurtzite are difficult to separate by EBSD, there is no reason why oxidation during sample preparation (e.g., polishing) should be localized to the beginning and the end of a cross section. Oxidation during production can be excluded because the reaction chamber is flooded with Ar for long periods of time before and after the material is actually produced. Also, the XRD analysis of these areas clearly indicates wurtzite (see Figure 1).

dx.doi.org/10.1021/am404454r | ACS Appl. Mater. Interfaces 2014, 6, 394−400

Figure 4 shows an interesting region within the marked white circle. The lowest misorientation detected between the large

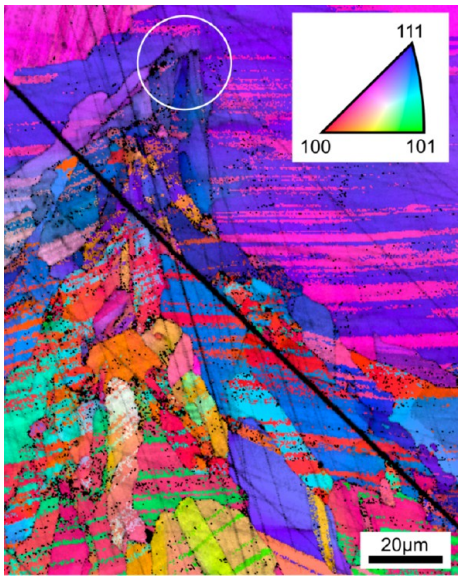

Figure 4. Combined IPF and IQ map of the area 2 framed in Figure 2 illustrating nucleation at a grain facet.

parent grain and the new grain is about 8°; i.e., upon nucleation there is no real large angle grain boundary (e.g., 15° or more) between the parent grain and the newly formed lattice. Only zincblende is indicated in the new grain. Figure 4 indicates that this nucleation is a frequently repeated process once it has been initiated. However, distinguishing between grain fragmentation during growth[4] and nucleation at the crystal face is not possible with certainty; the observed structure could also be a cut plane transecting a fragmented grain at an angle to its main growth direction. Figure 4 shows that the formation of new grains locally occurs in a very high frequency, and a continuous orientation change dividing one grain into several parts[4] is hardly observed. Many grains are observed near the nucleation site in Figure 4. The actual nucleus may be located outside the current cut plane. With every new nucleation step, a new nucleus with another misorientation of a few degrees is formed; i.e., the misorientation to the original grain increases.

Figure 5 illustrates a different type of growth. The main grain contains a lamellar twin system. The colors are assigned to the

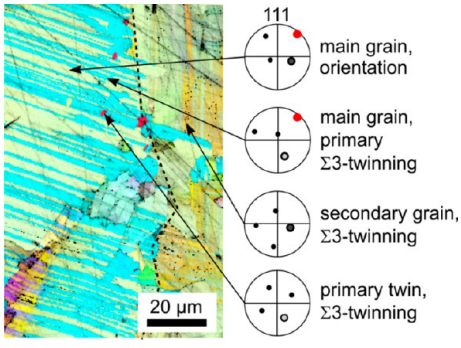

Figure 5. Combined IPF and IQ map of the area 3 framed in Figure 2 illustrating epitaxial growth during a change of the main growth direction of a grain. Twinning relationships are illustrated by 111-pole figures of selected orientations.

same inverse pole figure legend already presented above. The yellow lamellae are denoted as the main orientation which is in a Σ3-relationship to the blue lamellae which are denoted as the primary twin orientation. At the right side of the main grain, twins with another orientation (orange) are observed. The primary lamellar structure attributed to yellow and blue is no longer detected, although the former primary orientation (yellow) is still present. However, it is in a new Σ3-relationship to the orange orientation, i.e., to a new growth direction. The blue and orange orientations are in a Σ9-relationship, but appropriate interfaces are rarely observed. Once the new lamellar system is established, the old primary twin orientation no longer occurs. Although an explicit interface like a large-angle grain boundary is not detected between the two twin systems, the orange orientation will be considered as the primary twin of a new grain. The dashed black line in Figure 5 marks the boundary between the two lattice systems with their respective twin systems. By analogy, the small red lattice segments are primary twins of the former primary twins (blue).

The SEM micrographs in Figure 6 show large growth structures which are neither flat nor homogeneous but instead exhibit a notable topography. The thickness of the sample varies from 400 to 900 μm as shown in Figure 2. The structures at the growth front show a difference in altitude of up to 500 μm, suggesting widely varying, possibly temporarily fluctuating growth velocities during the process. Two discernible morphologies are observed: the hexagonally shaped pillars presented in Figure 6 and the more or less circular cones with their tips toward the growth front shown in Figure 7. The pillars are in some cases terminated by flat plateaus (see Figure 6a), with diameters of up to 200 μm and very thin structures of hexagonal shape frequently observed on them (see arrow in Figure 6b). Tipped pillars like the one in Figure 6c are also observed.

The circular cones are usually terminated by hexagonal tips where a distinctive step grows out of one hexagon segment (see Figure 7a and b). When these pillars join into more complex structures like the one presented in Figure 7d, intermediate stages occur (see Figure 7c). It may be assumed that both structures originate from very small nuclei near the initial substrate.

Figure 8a presents EBSD patterns obtained at the locations marked in the SEM micrograph in the middle: from the small hexagon (left) and from the plateau beneath the hexagon (right). The Kikuchi bands are the direct consequence of electron diffraction at the crystal lattice and form the EBSD pattern which in turn contains all the crystallographic information of the lattice; e.g., the bandwidth is directly correlated to the distance between lattice planes.

Figure 8b illustrates that both EBSD patterns share some Kikuchi bands and zone axes (highlighted in white), but a closer look reveals a number of separative details. The black lines highlight differing Kikuchi bands which are only attributable to either the cubic or the hexagonal structure. Relevant indexing parameters are presented to show that the hexagon is composed of wurtzite, while the plateau contains zincblende. The most significant commonality of the patterns is the location of the hexagonal $[000\bar{1}]$- and the cubic $[1\bar{1}1]$-zone axis and the attached Kikuchi bands, which indicates an epitaxial relationship between both phases. The same orientation relationship between the chemically similar hexagonal and cubic phases has also been described to occur

dx.doi.org/10.1021/am404454r | ACS Appl. Mater. Interfaces 2014, 6, 394−400

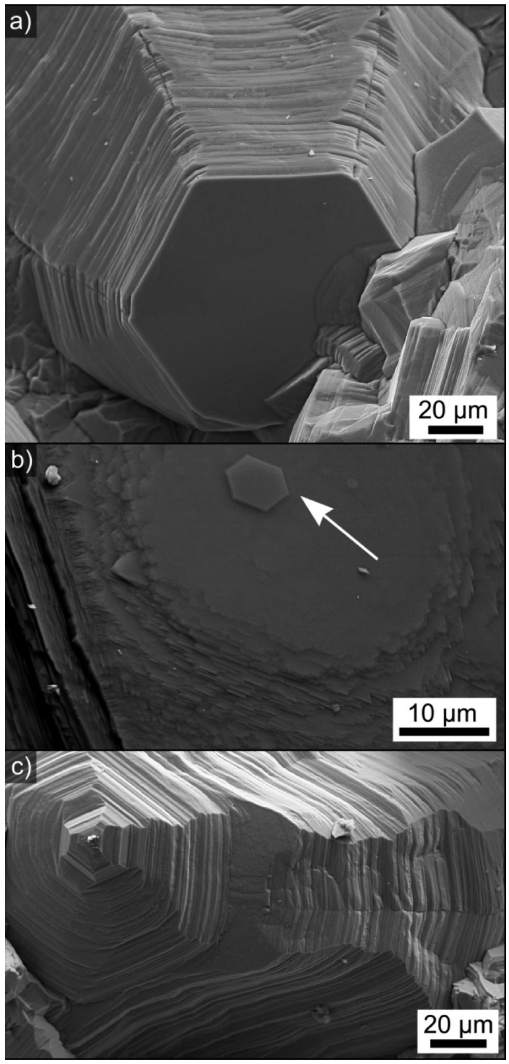

Figure 6. SEM micrographs of growth structures in the form of hexagonal pillars. (a) The pillars are terminated by flat plateaus with diameters of up to 200 μm. (b) Very thin structures of hexagonal shape frequently observed on the pillars. (c) Tipped pillars are also observed.

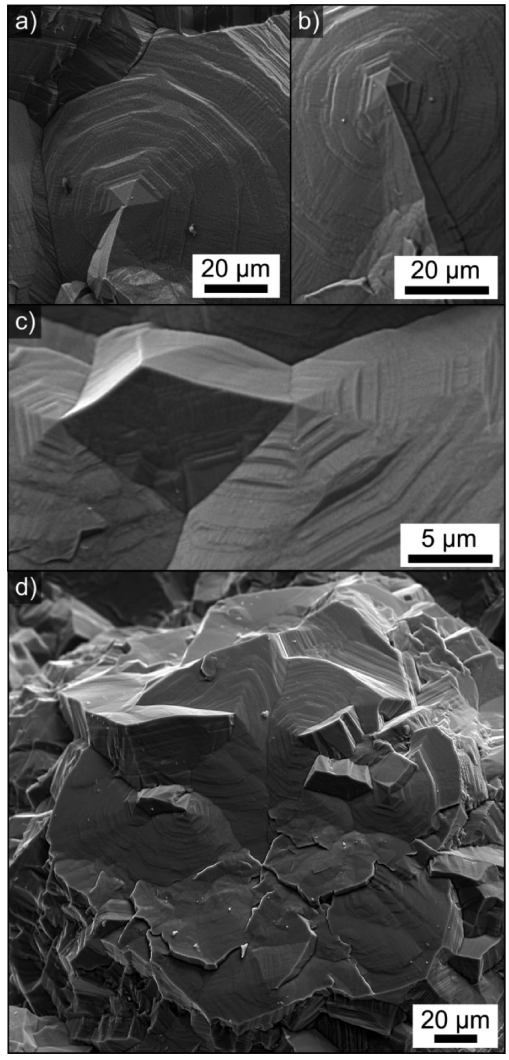

Figure 7. SEM micrographs of major growth structures. Circular cones are usually terminated by hexagonal tips from which a distinctive step grows out of one hexagon segment, (a) and (b). Intermediate stages (c) are formed when the pillars join into more complex structures (d).

in glass ceramics where hematite crystals transform to magnetite during annealing.[12]

The patterns in Figure 8 indicate that a ⟨0001⟩-direction (wurtzite) and a ⟨111⟩-direction (zincblende) of the respective phases are perpendicular to the plateau surface, confirming a ⟨111⟩-direction as the main direction of ZnS growth. Thus, the close-packed atomic layers of both phases are parallel to the plateau.

The SEM micrograph of an entire growth front plateau superimposed by the phase map of an EBSD scan of the area is presented in Figure 9a. The map shows that both wurtzite (red) and zincblende (green) occur in this area. This seems to contradict the XRD results in Figure 1b, but it should be noted that the information depth of EBSD has been stated to range from 5 to 50 nm,[13] while that of XRD may be calculated[14] to reach about 80 μm in ZnS. This confirms that notable amounts of wurtzite only form at the end of the process, while it is absent in the bulk, matching recent results.[4] Reliable phase discrimination in EBSD scans is only possible by considering the above-mentioned separative details between hexagonal and cubic EBSD patterns when building the material files. This problem is additionally enhanced by EBSD pattern superposition, which frequently occurs due to the thin twin lamellae.

Figure 9b presents an orientation map of the same EBSD scan highlighting specifically defined orientations. While wurtzite occurs in only one, zincblende occurs in two different orientations. All orientations deviate up to 10° from the defined values throughout the entire plateau, but always continuously instead of abruptly. The corresponding pole figures show that the *c*-axis of wurtzite is perpendicular to the plateau, while both zincblende orientations share a common {111}-lattice plane which is parallel to the plateau and the {0001}-plane of wurtzite, matching the results presented in Figure 8. The two zincblende orientations are rotated by 60° from each other around a ⟨111⟩-direction, indicating this is the same twinning of zincblende outlined above.

Free standing whiskers and tetrapods presented in Figure 10 often grow from the plateaus presented in Figure 6. Both structures only occur at the growth front in varying distribution and frequency. The step-like topography of the hexagon in Figure 10a is emphasized by the tilt of the plateau. Tetrapods

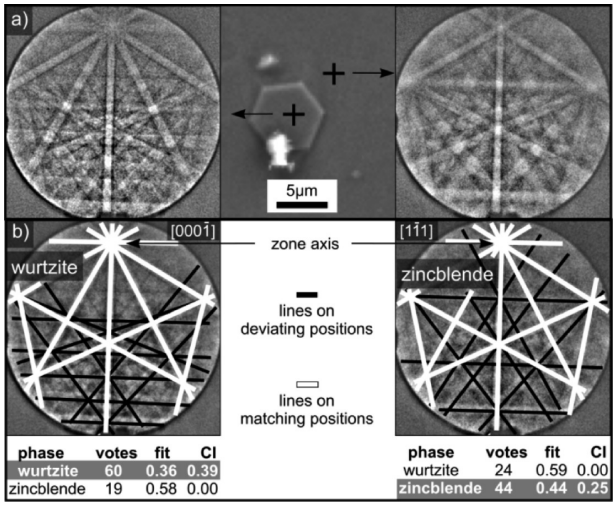

Figure 8. (a) Kikuchi patterns and detecting positions at the immediate growth front. (b) Indexing the patterns: common and differing Kikuchi bands are highlighted. The pattern from the hexagonally shaped plate is attributed to wurtzite, and the pattern from the plateau is indexed as zincblende. Relevant indexing parameters are presented.

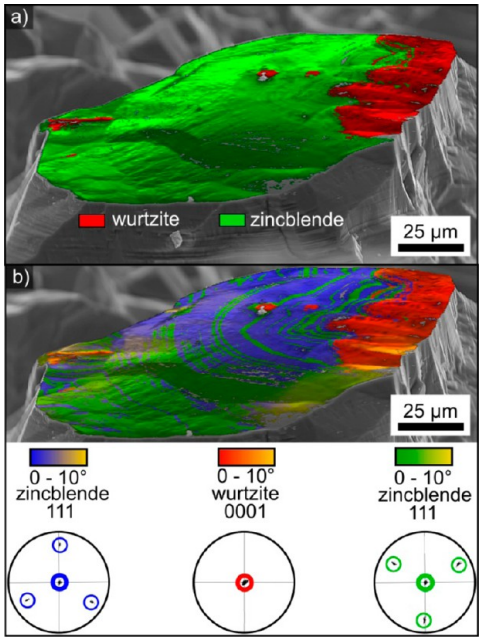

Figure 9. SEM micrograph of a pillar plateau superimposed by (a) the combined phase and IQ map and (b) the combined orientation and IQ map of an EBSD scan of the area. Pole figures visualize the individual orientations in the map.

with cubic centers and hexagonal arms have, e.g., been described for nanostructures in ZnS.[15]

EBSD patterns gained from flat faces of these ZnS nanostructures are indexable as wurtzite, while no indexable patterns could be obtained from the core of the tetrapods. An epitaxial orientation relation to the hexagonal structure they originate from is not observed. The high contrast particle in the SEM micrograph of Figure 8 is also a whisker on a wurtzite plate at the growth front viewed without sample tilting. ZnS whiskers with several morphologies grown under specific conditions, different from the CVD process used here, have

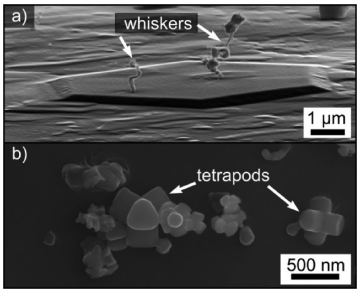

Figure 10. SEM micrographs of nanostructures which grow during process termination: (a) ZnS whiskers protruding from a hexagonally shaped face (sample tilted by 70°) and (b) cluster of tetrapods (no sample tilt).

already been studied in detail.[16−18] Other ZnS nanoparticles such as tubes, rods, or platelets condense from gases in areas of locally low temperatures.[16−19]

The material at the immediate growth front was deposited during the termination of the CVD process. This means that the heater is turned off abruptly, and the influx of H_2S, Ar, and subsequently Zn vapor is terminated. The main volume of the reaction chamber, however, is subject to a degree of inertia. In consequence further deposition occurs under dynamic and locally varying conditions. The concentration of reactants decreases quickly, although the cooling rate is low. It is plausible to assume that ZnS growth is ultimately terminated within 10 h because after this point the temperature in the reactor should be too low for Zn vapor to exist.

A comparable period with reversed gradients of temperature and concentration must be passed while starting the process. Experimental data toward this aspect, however, do not exist and are very difficult to obtain considering the industrial ZnS production. Special structures may grow during both process times of dynamical conditions. Studies of ZnS nanostructures show that the formation of wurtzite may occur at temperatures clearly below the equilibrium temperature.[17,18,20]

Taking the Gibbs free energy for zincblende and wurtzite from thermodynamic tables[5] and extrapolating the data of wurtzite down to the processing temperature using a second degree polynom, a ΔG value of only 4.5 kJ/mol is obtained at 680 °C which steadily increases to 23.3 kJ/mol at room temperature. Hence, the difference in the Gibbs free energy between both phases is very small under the supplied process conditions. It is well-known that phases not thermodynamically stable at the applied conditions are preferably formed in nanostructures. As discussed in refs 21 and 22, the conditions for the predominant formation of a metastable phase depend on the nucleation rates of the stable and the metastable phases. If the specific surface energy of the stable phase is higher than that of the metastable (high-temperature) phase, it might be thermodynamically advantageous to form nuclei of the metastable phase. It has been proposed in the literature that the difference in surface energy between two phases may lead to core-shell structures or end-selective growth,[23] i.e., at the growth front discussed here.

Comparing the phase compositions near the substrate, in the bulk and at the growth front, enables us to conclude that the detected wurtzite and the whiskers only grew under the described dynamic conditions and not in the main process period. Alternatively, a posteriori phase transition from wurtzite to zincblende would have to occur where the wurtzite at the substrate is stabilized in some way. If this were the case, one

would expect to find small amounts of untransformed wurtzite throughout the samples, which is not observed.

In the following, the observed mechanisms contributing to the grain structure in industrial CVD-ZnS will be discussed. It is helpful to keep in mind that the epitaxial deposition process is dominated by surface diffusion as shown in the case of CVD-diamond, which exhibits very similar effects in the microstructure.[24] A general kinetic selection with a broadening of the grains in the growth direction was already described for several CVD materials.[4,24,25] However, at least four mechanisms counteract the growth of large grains during the currently discussed process: twinning, development of new grain growth directions, grain fragmentation, and secondary nucleation.

Considering the epitaxial relationships between the cases of twinning and the coexistence of wurtzite and zincblende at the growth front, it can be concluded that the grains grow via the stacking of close-packed 111-layers. The formation of these layers probably occurs in the form of the stepped growth reported for CVD-diamond which is a similar material.[26] The stacking sequence, and subsequently the resulting phase, may also depend on energetic details, i.e., including the current environmental conditions such as the concentration of reactants as well as temperature and pressure.

Twinning can be considered as a kind of stacking fault and occurs without changing the orientation of the current {111}-plane at the growth front or of the {111}-plane polarity. Theoretical calculations for cubic face centered aluminum explicitly show that the surface energy for the symmetric tilt boundary in the case of a Σ3-twin orientation is nearly zero.[27] This has not yet been calculated for ZnS, but in principle it should lead to similar results. Even though Σ3-twinning occurs quite often in CVD-ZnS, it cannot introduce a lot of fault energy.

However, as the crystal orientations change during twinning, except for the twin plane, the side faces of grains include facets of twins, while the growth front plain remains homogeneous. This is observed in Figure 5 where the side face of the primary grain served as the substrate for the secondary grain. The latter additionally developed a new growth direction while continuing the main orientation of the primary grain with a new {111}-face as the new growth front. Consequently the new growth front has a different orientation in relation to the primary grain. The detailed reason or the point in time when the growth starts along a new direction is not yet clear. Important factors could be the density of faults and the facet size. As soon as a certain plateau size is reached at the growth front, the following layer may begin to grow while the base layer continues to grow in width. It is possible that several new steps begin their growth at different positions on the same plateau. If some dislocations are built into the base layer between these new steps, more energy should be required to build a complete layer. New faults and dislocations hence become more likely. This might lead to the grain fragmentation reported in ref 4 and observed in Figure 2. The observation in Figure 4, however, provides an additional explanation: if the energy for continuing a distorted lattice is higher than the nucleation energy of a nucleus with an orientation similar to the respective surface layer, the formation of a new nucleus would be preferred. Subsequent growth by the epitaxial deposition of new layers proceeds until one of the grain surfaces is large enough to allow the growth processes outlined above.

CONCLUSIONS

The industrial production of cubic CVD-ZnS is accompanied by the formation of hexagonal wurtzite during the dynamical conditions of process initiation and termination. Wurtzite does not affect the optical properties of the final material as it is removed during the post-production process and hence never occurs in an applied component. The analysis of the cubic and hexagonal phases of ZnS by EBSD is only possible by regarding certain separative details when building the material files and optimizing the phase discrimination. Under the stable conditions of the main process, cubic ZnS grows by the epitaxial deposition of 111-oriented layers. The large grain growth at the beginning of the CVD process includes the formation of pillars up to 400 μm high. Instead of forming single-crystalline grains, the previously described twinning and grain fragmentation as well as the newly proposed nucleation on grain facets and the change of the primary growth direction lead to the complex microstructure of industrial CVD-ZnS.

AUTHOR INFORMATION

Corresponding Author

*Tel.: (0049) 03641 948515. Fax: (0049) 03641 948502. E-mail: wolfgang.w@uni-jena.de.

Notes

The authors declare no competing financial interest.

ACKNOWLEDGMENTS

This work was funded by the Bundesministerium für Wirtschaft, BMWI (ZIM program KF2519702FK1).

REFERENCES

(1) Tran, T. K.; Park, W.; Tong, W.; Kyi, M. M.; Wagner, B. K.; Summers, S. J. *J. Appl. Phys.* **1997**, *81*, 2803−2809.
(2) Yu, P. Y.; Cardona, M. In *Fundamentals of Semiconductors: Physics and Materials Properties*, 3rd ed.; Springer: Berlin, Heidelberg, NY, 2005.
(3) McCloy, J.; Korenstein, R. *J. Am. Ceram. Soc.* **2009**, *92*, 1725−1731.
(4) Zscheckel, T.; Wisniewski, W.; Rüssel, C. *Adv. Funct. Mater.* **2012**, *22*, 4969−4974.
(5) Knacke, O.; Kubaschewski, O.; Hesselmann, K. In *Thermodynamical Properties of Inorganic Substances*; Springer: Berlin, Heidelberg, NY, 1991.
(6) Coster, D.; Knol, K. S.; Prins, J. A. *Z. Phys.* **1930**, *63*, 345−369.
(7) Medizadeh, V.; Mardix, S. *Acta Crystallogr.* **1986**, *C42*, 518−519.
(8) Alexander, E.; Kalman, Z. H.; Mardix, S.; Steinberger, I. T. *Philos. Mag.* **1970**, *21*, 1237−1246.
(9) Skinner, B. J.; Bethke, P. M. *Am. Mineral.* **1961**, *46*, 1382−1382.
(10) Rabadanov, M. K. *Kristallografiya* **1995**, *40*, 17−22.
(11) Field, D. P. *Ultramicroscopy* **1997**, *67*, 1−9.
(12) Wisniewski, W.; Harizanova, R.; Völksch, G.; Rüssel, C. *CrystEngComm* **2010**, *13*, 4025−4031.
(13) Schwartz, A. J.; Kumar, M.; Adams, B. L.; Field, D. P. In *Electron Backscatter Diffraction in Materials Science*, 2nd ed.; Springer: Berlin, Heidelberg, NY, 2009.
(14) Henke, B. L.; Lee, P.; Tanaka, T. J.; Shimabukuro, R. L.; Fujikawa, B. K. *At. Data Nucl. Data Tables* **1982**, *27*, 1−144.
(15) Wang, R.; Liu, W. *Thin Solid Films* **2012**, *522*, 40−44.
(16) Hao, Y.; Meng, G.; Wang, Z. L.; Ye, C.; Thang, L. *Nano Lett.* **2006**, *6*, 1650−1655.
(17) Moore, D.; Ronning, C.; Ma, C.; Wang, Z. L. *Chem. Phys. Lett.* **2004**, *385*, 8−11.
(18) Yin, L. W.; Bando, Y.; Zhan, J. H.; Li, M. S.; Goldberg, D. *Adv. Mater.* **2005**, *17*, 1972−1977.

(19) Meng, X. M.; Liu, J.; Jiang, Y.; Chen, W. W.; Lee, C. S.; Bello, I.; Lee, S. T. *Chem. Phys. Lett.* **2003**, *382*, 434−438.
(20) Prathap, P.; Revathi, N.; Subbaiah, Y. P. V.; Reddy, K. T. R. *J. Phys.: Condens. Matter* **2008**, *20*, 035205.
(21) Gutzow, I.; Avramov, I. *J. Non-Cryst. Solids* **1974**, *16*, 128−142.
(22) Avramov, I.; Gutzow, I. *Mater. Chem.* **1980**, *5*, 315−336.
(23) Milliron, D. J.; Hughes, S. M.; Cui, Y.; Manna, L.; Li, J.; Wang, L. W.; Alivisatos, A. P. *Nature* **2004**, *8*, 190−195.
(24) Liu, T.; Raabe, D.; Mao, W.; Zaefferer, S. *Adv. Funct. Mater.* **2009**, *19*, 3880−3891.
(25) van der Drift, A. *Philips Res. Rep.* **1967**, *22*, 267−288.
(26) Frenklach, M.; Skokov, S.; Weiner, B. *Nature* **1994**, *372*, 535−537.
(27) Hasson, G.; Biscondi, M.; Lagarde, P.; Levy, J.; Goux, C. *The Nature and Behaviour of grain boundaries*; Hsun, H., Ed.; The Metallurgical Society of AIME Proceedings; Plenum Press: New York - London, 1972.